# PCCP

Accepted Manuscript

This is an *Accepted Manuscript*, which has been through the Royal Society of Chemistry peer review process and has been accepted for publication.

*Accepted Manuscripts* are published online shortly after acceptance, before technical editing, formatting and proof reading. Using this free service, authors can make their results available to the community, in citable form, before we publish the edited article. We will replace this *Accepted Manuscript* with the edited and formatted *Advance Article* as soon as it is available.

You can find more information about *Accepted Manuscripts* in the Information for Authors.

Please note that technical editing may introduce minor changes to the text and/or graphics, which may alter content. The journal's standard Terms & Conditions and the Ethical guidelines still apply. In no event shall the Royal Society of Chemistry be held responsible for any errors or omissions in this *Accepted Manuscript* or any consequences arising from the use of any information it contains.

ROYAL SOCIETY OF CHEMISTRY

www.rsc.org/pccp

# Effect of Strain on the Electronic and Optical Properties of Ge/Si Dome Shaped Nanocrystals

Mahesh R. Neupane,*,† Rajib Rahman,‡ and Roger K. Lake*,†

*Department of Electrical and Computer Engineering, University of California, Riverside, CA 92521-0204, and Network for Computational Nanotechnology (NCN), Purdue University, West Lafayette, Indiana*

E-mail: mneup001@ucr.edu; rlake@ee.ucr.edu

**Abstract**

The effects of strain and confinement on the energy levels and emission spectra of dome-shaped, Ge-core/Si-shell nanocrystals (NCs) with diameters ranging from 5 to 45 nm are investigated with atomistic models. For NCs with base diameters ≥15 nm, the strain-induced increase in the energy gap is ∼ 100 meV. The increase in the energy gap is primarily the result of the downward shift in the occupied states confined in the Ge core. The fundamental energy gap varies from 960 meV to 550 meV as the NC diameter increases from 5 nm to 45 nm. Confinement and strain break the degeneracy of the lowest excited state and split it into two states separated by a few meV. For the smaller NCs, one of these states can be localized in the Si core and the other state can be in the Si cap. For diameters ≥ 20 nm, both of these states are localized in the Si cap. The electronic states are calculated using an atomistic $sp^3d^5s^*$ tight-binding model including spin-orbit coupling, and geometry relaxation is performed using a valence force field model.

*To whom correspondence should be addressed
†Department of Electrical and Computer Engineering, University of California, Riverside, CA 92521-0204
‡Network for Computational Nanotechnology (NCN), Purdue University, West Lafayette, Indiana



Physical Chemistry Chemical Physics Accepted Manuscript

Physical Chemistry Chemical Physics Accepted Manuscript

# Introduction and motivation

Aggressive scaling and the demand for high speed electronic and photonic devices have resulted in a large effort to understand carrier dynamics in heterostructure based nanostructures, such as InAs/GaAs,[1–3] CdTe/CdSe[4,5] and Ge/Si.[6–18] Ge/Si based nanostructures are of interest due to their compatibility with the existing silicon-based technology. Furthermore, Ge/Si nanostructures with various shapes (domes, wire, lens, and pyramids) have been fabricated and integrated in optical and electrical devices using advanced fabrication techniques such as molecular beam epitaxy (MBE),[19] self-assembly,[20–22] and chemical vapor deposition (CVD).[8] These devices exhibit size dependent characteristics and show potential for future devices such as thin-film field effect transistors,[7] flash memory,[8,10] DotFETs,[23] photodetectors,[24] solar cells,[25,26] and quantum computers.[15,16,27,28] Inter-level optical transitions in Ge/Si NCs have attracted interest due to the TYPE-II band alignment at the Ge and Si interface causing the holes and electrons to be spatially separated in the Ge and Si regions, respectively. There is significant effort to exploit these complex nanostructures to maximize the performance of future devices.[29–33]

Researchers have recently been successful in fabricating high quality Ge/Si NCs of different lateral dimensions and shapes in both single and multiple layers.[19,34–37] Of the various experimentally observed NC shapes, hut-shaped and dome-shaped Ge/Si NCs have unique electronic and optical properties.[38] Dome-shaped Ge/Si NCs with the curved bounding facets can relieve strain more efficiently compared to the hut, pyramid, or ring shaped NCs.[39]

Because of the 4.1% lattice mismatch between Si and Ge, the strain plays a key role in determining the energy levels.[40,41] Strain can shift both the conduction and valence states, alter the energy gap,[42,43] change the carrier dynamics,[12,14] modulate optical properties, and modify spin relaxation times.[44] In general, the strain distribution in Ge/Si NCs influences the shape and depth of the potential wells for electronic excitations, charge confinement, and carrier dynamics.[28]

Designing optoelectronic devices using Ge/Si NCs benefits from an atomistic model in

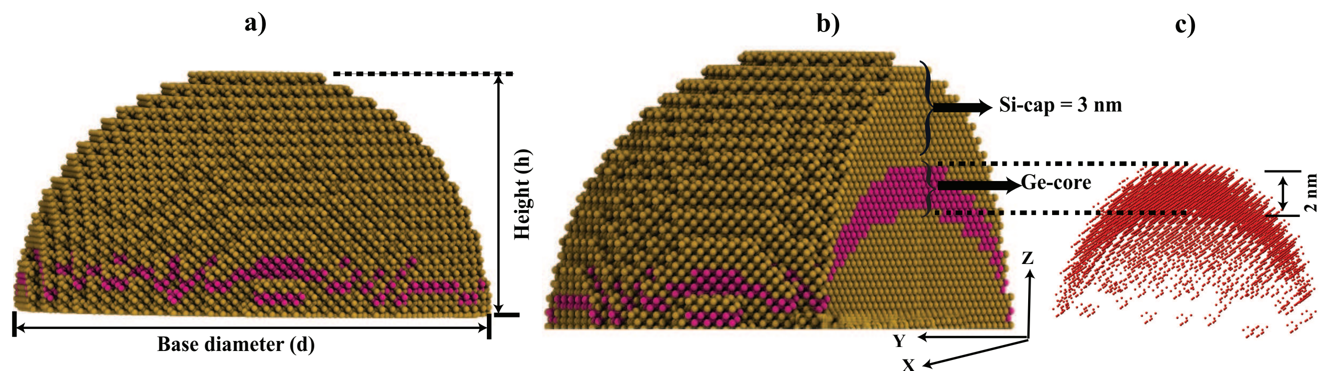


Figure 1: (Color online) One of the simulated Ge/Si dome-shaped NC structures with a 20 nm base diameter (b) and 10 nm overall height (h). a) Front view b) Cross-section view and c) Extracted Ge-core. The base diameters of the simulated structures varies from a minimum value of 5 nm to the maximum value of 45 nm. The NC height is fixed at 10 nm.

both the Ge-core and the surrounding Si regions. When evaluating the polarization dependent interlevel transitions, a fully atomistic treatment is necessary to capture atomistic effects at the Ge/Si interface that can mix electronic levels and modify the polarization.[45] Several theoretical works have supported experimental findings,[46,47] however, there are few large-scale, atomistic studies that include strain inhomogeneity while matching experimental shapes and sizes.[48] Lavichieve and et al. observed a huge discrepancy between experimental and theoretical findings in the optical and electrical properties of dome and pyramid shaped, Si-capped, Ge NCs embedded in the Si-matrix.[49] They attributed this discrepancy to their model's inability to realize the atomistic representation of the experimental structure. Recently, Usman et al. published an extensive theoretical study on III-V NCs highlighting the importance of strain and shape on the overall optoelectronic properties.[2,50–52] However, similar studies of the Ge/Si system are lacking.

The diameter and the aspect ratio (AR), the ratio of the height (h) to the base diameter (d), determine the overall stability of the NC.[30] A decrease in the aspect ratio corresponds to a morphological transition from a dome to an energetically favorable superdome resulting from excessive Ge deposition.[36,53,54] Recently, good control over the height of a Ge/Si NC system has been demonstrated with less control over the diameter.[55–59] This motivates our study of the diameter dependent properties of Ge/Si NCs. The atomistic structure of the



Physical Chemistry Chemical Physics Accepted Manuscript

Physical Chemistry Chemical Physics Accepted Manuscript

20 nm diameter NC is shown in Fig. 1. The NC cross-section in Fig. 1(b) shows the half-moon like Ge-core sandwiched between the two Si layers. The Ge core is extracted and illustrated in Fig. 1(c). This crescent shaped Ge-core has been observed experimentally by Lee et al.[53] Experimentally, the Si-capping layer is used not only to prevent Ge atoms from being oxidized during the control oxide growth,[8] but also to preserve the dome shape and size during growth.[60,61] Prior experimental studies of Ge/Si heterostructures demonstrated sharp interfaces with minimal intermixing.[62,63] We leave the investigation of intermixing at the interface for a future study. The Ge and Si interfaces are inhomogeneously strained due to the lattice mismatch between Si and Ge.

We present a systematic computational study of the confinement and strain effects on the electrical and optical properties of Ge/Si dome-shaped NCs with crescent-shaped Ge-cores. The spatially resolved strain distribution is calculated atomistically throughout the structure. The strain modulated energy-level and energy gap shifts are determined. Optical transition rates are calculated. The effect of the lattice strain on the electronic properties of dome-shaped Ge/Si NCs is analyzed by making one-to-one comparisons of device properties calculated from strained and unstrained systems. Electronic structure calculations are performed with NEMO3D.[64] The accuracy of the models have been verified by comparison with experimental data in SiGe systems,[65] strained InGaAs quantum dots,[52] a single impurity in Si FinFets[66–68] and Si-based single electron transistors.[69,70]

# Structure and Method

The growth direction of the NCs is the [001] direction. The heights of all NCs are fixed at 10 nm, and the diameters are varied from 5 nm to 45 nm. The thicknesses of the base, core, and cap at the center of the NCs are fixed and they taper towards the perimeter as shown in Figs. 1(b,c). At the NC center, the thickness of the base, core, and cap are 5 nm, 2 nm, and 3 nm, respectively.

Physical Chemistry Chemical Physics Accepted Manuscript

Geometry relaxation uses an atomistic valence force field (VFF) model with additional interaction terms included in the Keating model, and the minimization procedure employs the conjugate gradient technique.[64,71–74] This approach has been extensively used to model strain in complex quantum dots and other nanostructures, and it has qualitatively compared well with the various experimental data.[7,65,67–69] During relaxation, the $z$-position of the bottom layer of the Si atoms is fixed, and they are free to move in $x$ and $y$. Free boundary conditions are applied at all other surfaces. These boundary conditions approximate those during growth of a NC on an amorphous $SiO_2$ layer as is done in NC memory applications.[8,10]

Once the structure is relaxed to its minimum energy configuration, the strain components for all of the atomic sites are calculated using the formalism introduced by Pryor and co-workers.[71] In the relaxed structure, each atom is surrounded by 4 nearest neighbors at positions $\mathbf{R}_j$ in a strained tetrahedron. The strained tetrahedron edges given by the difference vectors $\mathbf{R}_{i,j} = \mathbf{R}_j - \mathbf{R}_i$ are related to the unstrained tetrahedron edges $\mathbf{R}^0_{i,j} = \mathbf{R}^0_j - \mathbf{R}^0_i$ by the strain tensor as

$$\begin{bmatrix} \mathbf{R}_{1,2} & \mathbf{R}_{2,3} & \mathbf{R}_{3,4} \end{bmatrix} = \begin{bmatrix} \mathbf{I} & + & \mathbf{E} \end{bmatrix} \begin{bmatrix} \mathbf{R}^0_{1,2} & \mathbf{R}^0_{2,3} & \mathbf{R}^0_{3,4} \end{bmatrix} \tag{1}$$

where each column $\mathbf{R}_{i,j}$ is a column vector of the $x, y, z$ components of the vector $\mathbf{R}_{i,j}$. $\mathbf{I}$ is the identity matrix and $\mathbf{E}$ is the strain tensor. After solving Eq. (1) for the strain tensor, the resulting in-plane strains ($E_{xx}$ and $E_{yy}$) and the out-of-plane strain ($E_{zz}$), at each atomic site, are used to calculate the hydrostatic strain $\epsilon_H = E_{xx} + E_{yy} + E_{zz}$ and the biaxial strain $\epsilon_b = E_{xx} + E_{yy} - 2E_{zz}$.

The electronic structure is calculated by solving for the eigenvalues and eigenstates of an atomistic tight-binding Hamiltonian with a 20-band $sp^3d^5s^*$ basis including spin-orbit coupling (SO) as implemented in NEMO3D.[75] The SO splitting of the split-off hole band in bulk Si and Ge is 40 and 300 meV, respectively. Without the SO interaction, the bulk valence bands have 3-fold orbital degeneracy, with each band at $\Gamma$ being a pure bonding $|p_x\rangle$,

Physical Chemistry Chemical Physics Accepted Manuscript

$|p_y\rangle$, or $|p_z\rangle$ state. The SO interaction reduces the orbital degeneracy to 2-fold, and it also mixes the orbitals. Even in bulk, one must include the SO interaction to get a qualitatively correct valence band for these semiconductors. In our system, the valence band becomes quantized states localized in the Ge core. The SO interaction qualitatively changes the level spacing and orbital composition of these levels.

The energies of the dangling bonds at the surface are increased by 20 eV to move the surface states away from the low-energy interior states of interest around the energy gap. These boundary conditions mimic the physical passivation of dangling bonds with H atoms, and they are described in detail in Refs.[76,77] They have been used extensively on nanocrystals, quantum wells, and nanowires.[65,66,78] The largest simulated NC contains 745176 atoms. With 20 orbitals per atom (10 orbitals $\times$ 2 spins), the total size of the basis is $1.4903 \times 10^7$, however the Hamiltonian is very sparse. The eigenvalues and eigenstates are solved using the Lanczos algorithm.[64] For the smaller NCs with diameters $\leq$ 20 nm, a block-Lanczos algorithm was also used for energies near the energy gap to ensure that no eigenenergies were missed.[79]

In order to quantify the strain contribution to the electronic and optical properties, the eigenenergies and wave functions are calculated twice, once using the tight-binding parameters of the relaxed structure, and once using the tight-binding parameters of the un-relaxed structure. For the un-relaxed structure, bulk Si and Ge tight-binding parameters are used, and the Si-Ge interface is treated using average values in a virtual crystal type approximation. Calculations of the electronic states in the un-relaxed and relaxed structures will be referred to as the un-strained and strained calculations, respectively. The unstrained calculations used the tight binding parameters for bulk Si and Ge described in Ref.[80] Calculations of the strained structures used modified tight-binding parameters[81] that incorporate changes in the bond length and bond angle on the nearest neighbor matrix elements and also include modification to the on-site orbital energies that lift orbital degeneracy in the presence of strain. The resulting wavefunctions and energy levels are used to determine other device related parameters such as energy gaps, momentum matrix elements, and optical transition

rates.[52,82]

The spontaneous emission rate $\Gamma(\omega)$ between an excited state and the ground state is calculated using Fermi's golden rule,

$$\Gamma(\omega) = \frac{e^2}{\epsilon_o \hbar^2 m_o^2 \pi c^3} \hbar\omega_{if} |\langle i|P_\nu|f\rangle|^2 \tag{2}$$

where, $e$ is the electron charge, $m_o$ is the bare electron mass, $\epsilon_o$ is the absolute dielectric permittivity of a vacuum, $c$ is the speed of light, $P$ is the momentum operator, $\nu$ is the polarization, $|i\rangle$ is the initial state, $|f\rangle$ is the final state, and $\hbar\omega_{if}$ is their energy difference. As part of the analysis, we define the envelope function at each atomic site $n$,

$$C_n{}^2 = \sum_{i=1}^{20} |\psi_{n,i}|^2 \tag{3}$$

where $|\psi_{n,i}|^2$ is the probability density of orbital $i$ at atomic site $n$. The envelope functions for the initial state $C^i$ and final state $C^f$ are then used to calculate the spatial overlap of the two wavefunctions as,

$$\text{Overlap} = |\sum_{i=1}^{N} C_n{}^i \cdot C_n{}^f|^2 \tag{4}$$

where $N$ is the total number of atoms in the structure.

# Results and Analysis

## Strain characteristics

The strain components at each atomic site are calculated using Eq. (1). The in-plane strain $E_{xx}$ and the out-of-plane strain $E_{zz}$ plotted in the [001] direction through the center of the NC are shown in Fig. 2(a,b) for 3 different diameter NCs. The positive and negative strain values correspond to tensile and compressive strain, respectively. There is a general trend of an abrupt change in $E_{xx}$ and $E_{zz}$ while passing through the Si / Ge interfaces at the bottom



Physical Chemistry Chemical Physics Accepted Manuscript

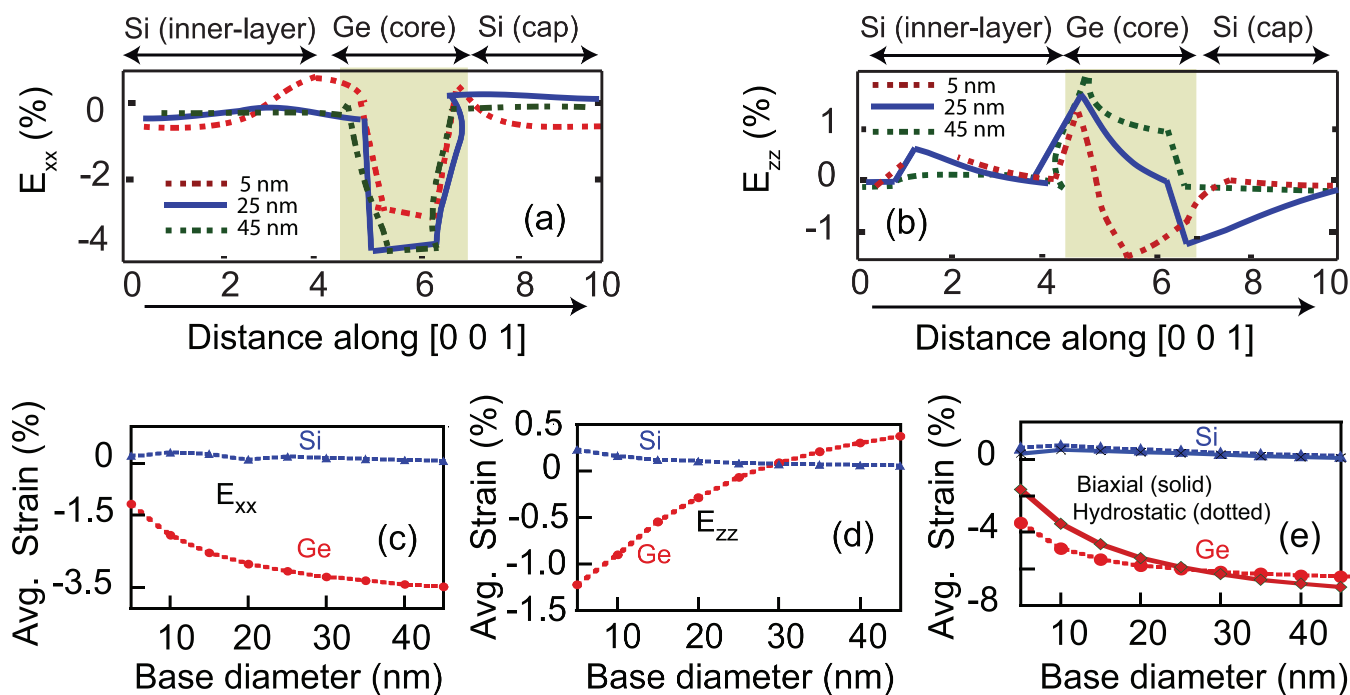


Figure 2: (Color online) (a) In-plane strain $E_{xx}$ and (b) out-of-plane strain $E_{zz}$, plotted along the [001] direction through the center of the NCs. The white and grey backgrounds correspond to the Si and Ge regions, respectively. The three different diameters are indicated in the legends. (c) Average in plane strain $\langle E_{xx} \rangle$ of the Ge and Si atoms. (d) Average out of plane strain $\langle E_{zz} \rangle$ of the Ge and Si atoms. (e) Average biaxial (solid line) and hydrostatic (dotted line) strain of the Ge and Si atoms, as a function of base diameter.



Physical Chemistry Chemical Physics Accepted Manuscript

and top of the Ge core. Since the Ge lattice constant is greater than the Si lattice constant, the Ge-core layer is compressed parallel to the interface giving negative values for $E_{xx}$ and $E_{yy}$. $E_{zz}$ becomes positive in order to maintain the Poisson ratio.

For the smaller NCs, the Ge atoms are, on average, compressed in all 3 directions as shown in the plots of the average strain in Figs. 2(c,d). In these plots, the values of the strain have been averaged over all of the Ge atoms and all of the Si atoms in the NC. Because of the high curvature of the Ge region in the smaller NCs, the physical distinction between $E_{xx}$ and $E_{zz}$ becomes blurred since the Ge atoms curve around the Si base. Once the base diameter becomes larger than 30 nm, the average strain takes on the character expected for a planar structure with $\langle E_{xx} \rangle < 0$ and $\langle E_{zz} \rangle > 0$. The average hydrostatic and biaxial strain in the Ge region is always negative as shown in Fig. 2(e). The average hydrostatic strain is 3.8% for a 5 nm NC and increases to 6% for a 45 nm NC. Due to the relatively large Si base region, the strain averaged over all of the Si atoms is small.

Iso-surface plots of the hydrostatic and biaxial strain of the Ge/Si NCs are shown for the smallest (5 nm), medium (25 nm), and largest (45 nm) diameter NCs in Fig. 3. The cross-sectional plane is taken through the NC center. For the smallest 5 nm diameter NC with an AR of 2, the local hydrostatic and biaxial strain distribution in the Ge and Si regions are the most inhomogeneous. The Si base, immediately underneath the Ge core, experiences the largest hydrostatic strain of 1.2% of all of the NCs. Conversely, the magnitude of the hydrostatic strain in the Ge core is the least among all of the NCs. In this smallest NC, the magnitude of the strain is shared most equally between the Si and Ge regions. As the diameter increases, and the volume of the Si base becomes much larger than the volume of the Ge core, the NC more resembles a planar heterostructure, and the strain becomes more localized in the Ge region. The general trend in the strain distribution is consistent with other theoretical and experimental results for similar lattice mismatched systems.[44,60,62]

Physical Chemistry Chemical Physics Accepted Manuscript

Physical Chemistry Chemical Physics Accepted Manuscript

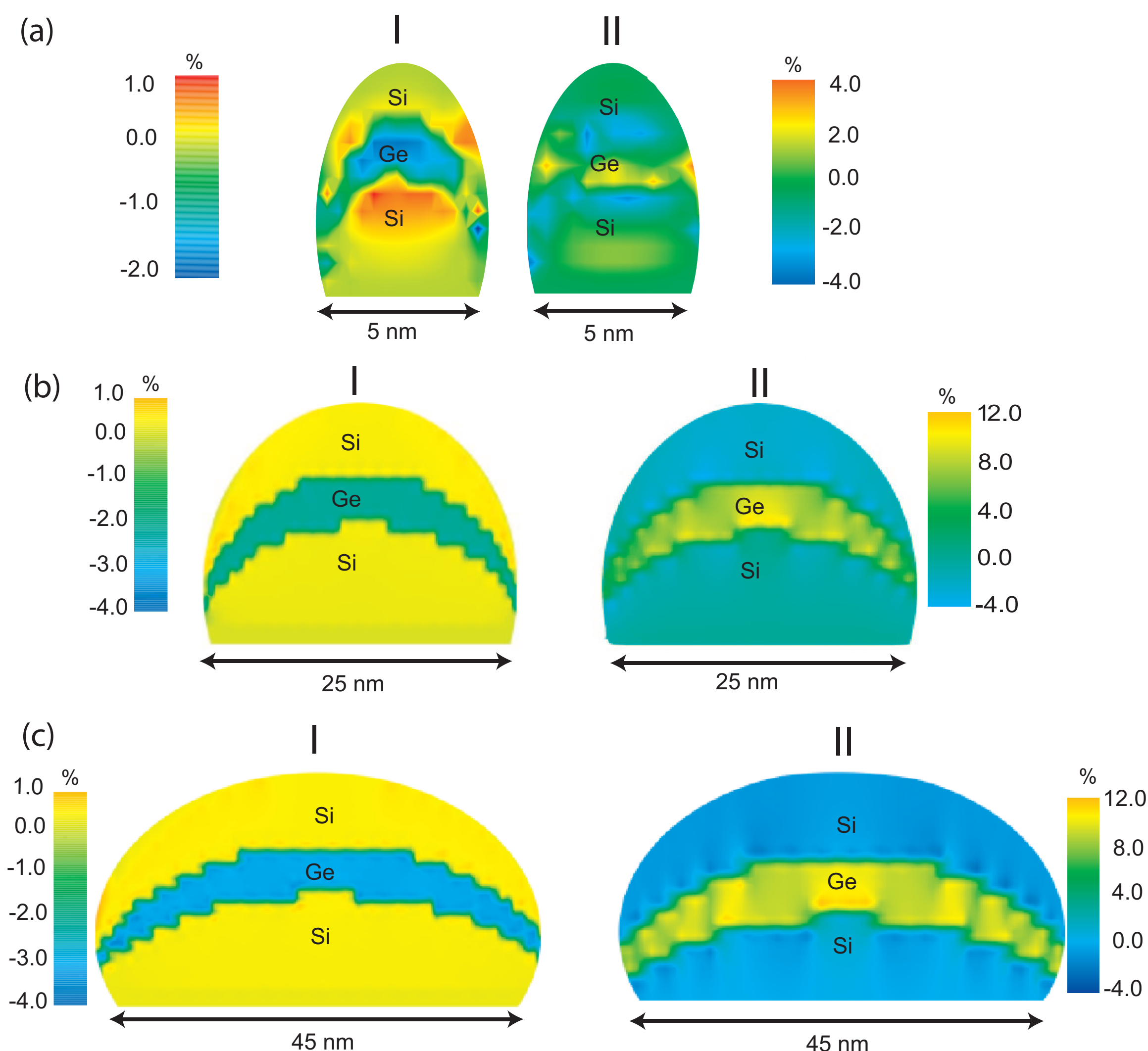


Figure 3: (Color online) Isosurface plots of the hydrostatic (I) and the biaxial (II) strain in a (100) plane cross-section through the NC center for the (a) smallest (5 nm), (b) intermediate (25 nm), and (c) largest (45 nm) dome-shaped Ge/Si NCs. The plane cuts through the Ge/Si interface at the center of the $x - y$ plane. The horizontal scales for the intermediate (b) and the largest (c) NCs are reduced by a factor of 2.

Physical Chemistry Chemical Physics Accepted Manuscript

## Electronic Properties

A schematic illustration of the energy levels and their spatial location in the Ge/Si NCs is shown in Fig. 4. Bulk Si and Ge form a type-II energy level alignment. The valance band offset of 0.70 eV creates a deep potential well in the Ge-core region which strongly localizes the occupied valence states of the NC. The unoccupied excited states localize in the Si base and in the Si cap. Whether an excited state is in the base or the cap depends on the size of the NC and the strain. The energy splitting of $\leq$ 15 meV between the three excited states $E_0$, $E_1$ and $E_2$ is small. Optical transitions that will be analyzed are shown.

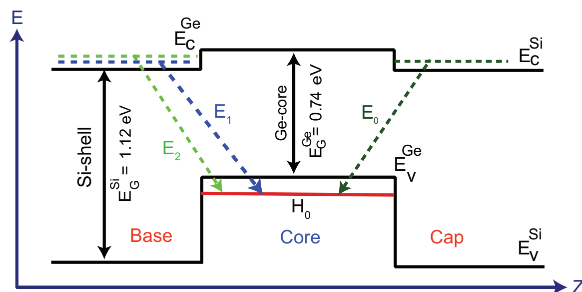


Figure 4: (Color online) Energy levels and optical transitions between the highest occupied state in the Ge core and the excited states in the Si base and cap.

To obtain insight into the energy and positions of the wavefunctions as a function of NC diameter and strain, we plot in Fig. 5 the colored iso-surfaces of the probability densities corresponding to the energies $H_0$, $E_0$, $E_1$, and $E_2$ for both the strained and unstrained NCs. The magnitude of the momentum matrix elements between the highest occupied level $H_0$ and first three excited states $E_0$, $E_1$ and $E_2$ are a few orders of magnitude larger than those between the second highest occupied level $H_1$ and $E_0$, $E_1$ and $E_2$. Hence, our study only focuses on these lowest-energy and more optically favorable transitions. For all of the NCs, with or without strain, the wavefunction $\psi_{H_0}$ of the highest occupied state is localized in the Ge core. The strain only lowers its energy level. The energy differences between the highest 3 occupied states of the strained (unstrained) NCs are 5 (3) meV for the largest NC and 50 (25) meV for the smallest NC.

The quantum confinement and strain both lift the degeneracy of the lowest excited state.

In all cases, with or without strain, the lowest excited state is non-degenerate. For the strained NCs, the first two excited states differ in energy by 2 - 4 meV with the maximum difference of 4 meV occuring in the 15 nm diameter NC. For the unstrained NCs, the energy splitting of the two lowest excited states is 1 meV. Thus, the strain enhances the splitting of the lowest excited state by a factor of 2 to 4. These values are similar or slightly larger than the splitting in strained GeSi/Si/GeSi QWs,[9] GeSi QDs[11] and disordered Si QD's,[18]and within the energy resolution limits of the advanced techniques like photon assisted tunneling.[83] This energy splitting of the excited states in a Ge/Si NC was observed experimentally for a Ge NC of height $\sim$ 2 nm and base diameter of $\sim$ 10 nm, sandwiched between two strained Si-layers.[84] The meV energy differences arise from the breaking of the bulk Si X-valley degeneracy due to the quantum confinement, and they are consistent with earlier studies of confined Si structures using both atomistic and analytical models.[9,18,65,67,78,85] These small energy level splittings have been of interest primarily for applications in quantum computing.

As the NC diameter increases from 10 nm to 25 nm, the localization of the excited states move. Consider the two lowest, nearly-degenerate excited states of the strained NCs. In the 10 nm NC, $\psi_{E_0}$ is localized in the Si base, and $\psi_{E_1}$ is localized in the Si cap. At 15 nm, $\psi_{E_0}$ and $\psi_{E_1}$ are both localized in the base, and at 25 nm, they are both localized in the cap. They both remain localized in the cap for all larger diameters. A similar switching between cap and base occurs in the unstrained NCs, however, the positions of $\psi_{E1}$ and $\psi_{E2}$ are the opposite of those in the strained NCs. For both the strained and unstrained NCs, the lowest two excited states reside in the cap for diameters $\geq$ 25 nm. The third level is about 7 meV above the first two for the larger NCs and only 1 meV above the second level for the 10 nm strained NC. The excited state wavefunctions in the cap have a larger spatial overlap with the occupied wavefunction in the Ge core than do the excited state wavefunctions in the base. This property affects the optical matrix elements.

To understand the effects of strain and confinement on the fundamental energy gap, the



Physical Chemistry Chemical Physics Accepted Manuscript

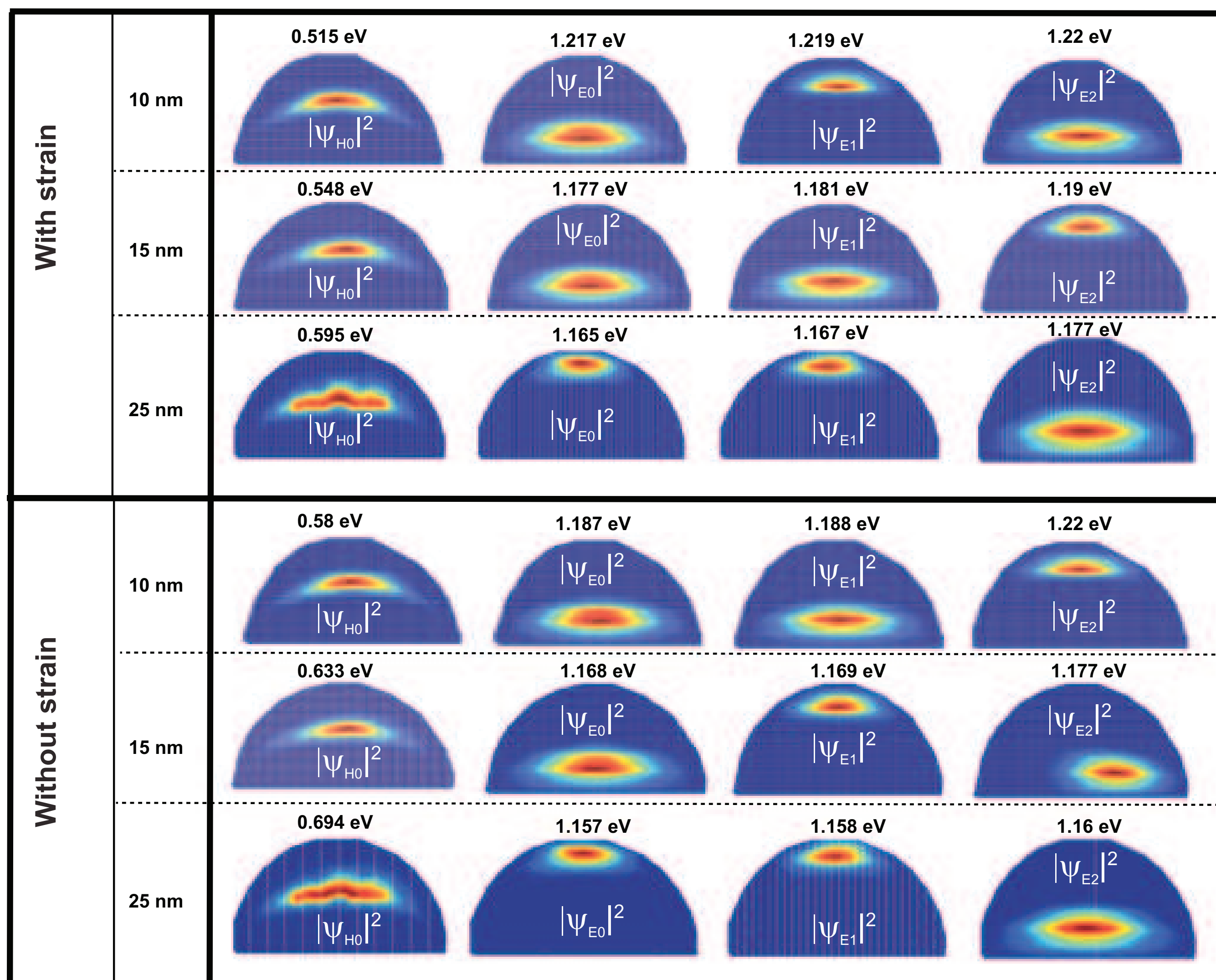


Figure 5: (Color online) Cross sections of the orbitals of the highest occupied state $H_0$ and the three lowest excited states, $E_0$, $E_1$, and $E_2$, for diameters of 10, 15 and 25 nm. The first three rows are calculated with strain and the lower three rows are calculated without strain. The corresponding energies associated with each state are labeled.



Physical Chemistry Chemical Physics Accepted Manuscript

individual energy levels and the fundamental energy gaps are plotted versus diameter for both the strained and unstrained NCs. The energy difference between the lowest excited state $\psi_{E0}$ and the highest occupied state $\psi_{H0}$ is defined as the energy gap $E_g$, and it is plotted in Fig. 6(a) as a function of the base diameter. The change in the $E_g$ with diameter is primarily the result of the change in the occupied state energy $H0$ with diameter. Confinement and compressive strain work together to lower the energy of the occupied state in the Ge core. For the smaller NCs $\leq$ 15 nm diameter, the confinement energy is larger than the strain energy. Beyond 15 nm, the strain energy dominates. The strain induced shift in $E_g$ for the smallest NC is 35 meV and it reaches a maximum value of 128 meV for the largest NC. The plot of the strain-induced shifts of the individual energy levels given in Fig. 6b, shows that the strain-induced increase in the energy gap is dominated by the strain-induced lowering of the occupied state localized in the Ge core. The strain lowers the eigenenergies of the highest occupied states $H_0$ by 38 meV in the 5 nm NC and by 120 meV in the 45 nm NC. These values were compared to the predictions of deformation potential theory using the average strain components described in the previous section and the deformation potentials from Ref.[86] The deformation potential theory lowers the energies of the highest occupied states of the 5 nm and 45 nm NCs by 45 meV and 100 meV, respectively, which is consistent with the above values of 38 meV and 120 meV. The effect of strain on the energies of the excited states localized in the Si base and cap is relatively small compared to its effect on the energies of the occupied states localized in the Ge core. For diameters greater than 20 nm, the strain raises the lowest excited state energy $E_0$ by about 10 meV.

## Optical Properties

The closely spaced excited states with energy spacing less than 15 meV can all contribute to the overall optical emission intensity.[2] The interlevel emission transition rate $\Gamma(\omega)$ is a function of the transition energy and the momentum matrix element. Since the initial and final wavefunctions are localized in different regions of the NC, some of the diameter



Physical Chemistry Chemical Physics Accepted Manuscript

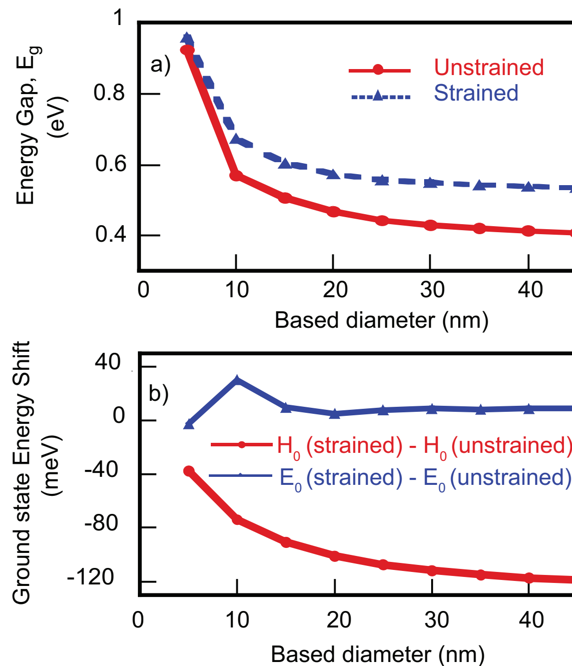


Figure 6: (Color online) Electronic states of dome-shaped Ge/Si NC as a function of base diameter, (a) Energy gap ($E_g$) for unstrained (solid line) and strained (broken line) case, and (b) Strain induced shift in the occupied state ($H_0$) and the excited state ($E_0$) energies.

dependent trends of $\Gamma(\omega)$ can be understood by considering the overlap of the occupied and excited state wave function envelopes. Fig. 7(a) shows the wave function overlap between the occupied state ($\psi_{H_0}$) and first three excited states ($\psi_{E_0}$, $\psi_{E1}$ and $\psi_{E_2}$) for the strained NCs calculated from Eq. (4). The wave function overlaps for the smallest Ge/Si NC are around 0.1. For the smallest NCs, $\psi_{E_0}$ is localized in the Si base. As the base size increases, $\psi_{E_0}$ moves away from $\psi_{H_0}$ in the Ge core, and the overlap decreases. At 20 nm, $\psi_{E_0}$ shifts from the Si base to the Si cap where it stays for all larger diameters. Therefore, as the diameter increases from 20 nm, the overlap is a smooth function of diameter and slightly decreases. The abrupt jumps in the wavefunction overlap moving from one diameter to the next result from the electronic state switching from the base to the cap or vice-versa. This also explains why, in the 15 nm NC, the overlap of $\psi_{E_2}$ with $\psi_{H_0}$ is larger than that of $\psi_{E_0}$ or $\psi_{E_1}$ with $\psi_{H_0}$. This is the one diameter where $\psi_{E_2}$ is localized in the cap and $\psi_{E_0}$ and $\psi_{E_1}$ are localized in the base.

The transition rates $\Gamma(\omega)$ between the first three excited states, $E_0$, $E_1$ and $E_2$, and



Physical Chemistry Chemical Physics Accepted Manuscript

Physical Chemistry Chemical Physics Accepted Manuscript

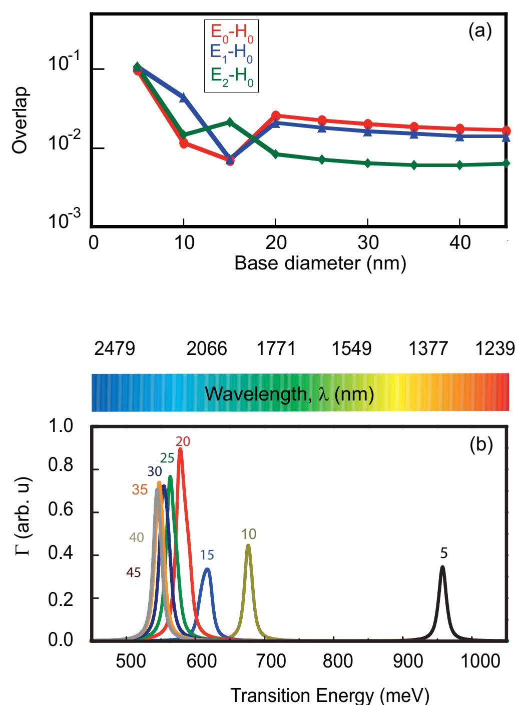


Figure 7: (Color online) Optical Properties of dome-shaped Ge/Si NCs as a function of base diameter (a) Wave function overlap between first three excited states ($E_0$, $E_1$, and $E_2$) and the ground state ($H_0$), and (b) Optical intensities between the the ground state $H_0$ and the excited states $E_0$, $E_1$, and $E_2$. For all the calculated transition intensities, Lorentzian broadening functions with the width of 10 meV are applied.

the ground state $H_0$ for in-plane polarization are calculated using Eq. (2). The discrete spectrum is convolved with a 10 meV Lorentzian broadening function and plotted in Fig. 7(b). For the smallest 5 nm NC, the rate between the highest occupied state and the lowest excited state dominates, and the peak energy (wavelength) associated with this transition lies at 960 meV ( 1292 nm). As the diameter is increased, the transition spectrum red-shifts following the trend in the energy gap and reaches a minimum of approximately 550 meV for NC diameters $\geq$ 25 nm. For these larger NCs, the magnitude of the emission rate is approximately two times larger than that of the 5 nm NC. This enhancement results from an increased magnitude of the momentum matrix elements between the initial and final states.

## Conclusion

Dome-shaped Ge-core/Si-shell nanocrystals with crescent shaped Ge cores and base diameters ranging from 5 nm to 45 nm have been simulated atomistically to determine the effect of quantum confinement and strain on the electrical and optical properties. Strain and confinement work together to lower the occupied state energies in the Ge core. Strain increases the energy gap by approximately 100 meV for NCs with base diameters greater than 15 nm, and the increase is a result of the downward shift of the occupied state in the Ge core. Confinement and strain break the degeneracy of the lowest excited state and split it into two states separated by a few meV. In the smaller NCs with base diameters below 15 nm, one of the states can be in the base and the other in the cap. For diameters $\geq$ 20 nm, the two lowest excited states are localized in the Si cap for both the strained and unstrained NCs. The fundamental energy gap and emission spectrum varies from 960 meV for the 5 nm NC to 550 meV for the largest NC with most of the variation occurring between 5 nm and 20 nm.

**Acknowledgements**

We thank Dr. Gerhard Klimeck and NCN/nanohub.org for providing NEMO3D for this



Physical Chemistry Chemical Physics Accepted Manuscript

research. We also thank Dr. Jianlin Liu, Dr. Huimei Zhou, Dr. Timothy Boykin, Dr. Somaia Sarwat Sylvia, Gen Yin, and Darshana Wickramaratne for useful discussions. This work was supported in part by the National Science Foundation (NSF) under Award No. DMR-0807232 and the Department of Education GAANN fellowship.

Physical Chemistry Chemical Physics Accepted Manuscript

Physical Chemistry Chemical Physics Accepted Manuscript

## References


1. Yan, X.; Zhang, X.; Ren, X.; Lv, X.; Li, J.; Wang, Q.; Cai, S.; Huang, Y. Formation Mechanism and Optical Properties of InAs Quantum Dots on the Surface of GaAs Nanowires. *Nano Letters* **2012**, *12*, 1851–1856.

2. Usman, M.; Tasco, V.; Todaro, M. T.; Giorgi, M. D.; Reilly, E. P. O.; Klimeck, G.; Passaseo, A. The polarization response in InAs quantum dots: theoretical correlation between composition and electronic properties. *Nanotechnology* **2012**, *23*, 165202.

3. Yu, Y.; Li, M.-F.; He, J.-F.; He, Y.-M.; Wei, Y.-J.; He, Y.; Zha, G.-W.; Shang, X.-J.; Wang, J.; Wang, L.-J. et al. Single InAs Quantum Dot Grown at the Junction of Branched Gold-Free GaAs Nanowire. *Nano Letters* **2013**, *13*, 1399–1404.

4. Smith, A. M.; Mohs, A. M.; Nie1, S. Tuning the optical and electronic properties of colloidal nanocrystals by lattice strain. *Nature Nanotechnology* **2008**, *4*, 56 – 63.

5. Mahadevu, R.; Yelameli, A. R.; Panigrahy, B.; Pandey, A. Controlling Light Absorption in Charge-Separating Core/Shell Semiconductor Nanocrystals. *ACS Nano* **2013**, *7*, 11055–11063.

6. Lauhon, L. J.; Gudiksen, M. S.; Wang, D.; Lieber, C. M. Epitaxial core-shell and core-multishell nanowire heterostructures. *Nature* **2002**, *420*, 57–61.

7. Liang, G.; Xiang, J.; Kharche, N.; Klimeck, G.; Lieber, C. M.; Lundstrom, M. Performance Analysis of a Ge/Si Core/Shell Nanowire Field-Effect Transistor. *Nano Letters* **2007**, *7*, 642–646.

8. Li, B.; Liu, J.; Liu, G. F.; Yarmoff, J. A. Ge/Si heteronanocrystal floating gate memory. *Applied Physics Letters* **2007**, *91*, 132107.

9. Friesen, M.; Chutia, S.; Tahan, C.; Coppersmith, S. N. Valley splitting theory of SiGe/Si/SiGe quantum wells. *Phys. Rev. B* **2007**, *75*, 115318.

Physical Chemistry Chemical Physics Accepted Manuscript


10. Lu, J.; Zuo, Z.; Chen, Y.; Shi, Y.; Pu, L.; Zheng, Y. Charge storage characteristics in metal-oxide-semiconductor memory structure based on gradual $Ge_{1-x}Si_x$/Si hetero-nanocrystals. *Applied Physics Letters* **2008**, *92*, 013105.

11. Friesen, M.; Coppersmith, S. N. Theory of valley-orbit coupling in a Si/SiGe quantum dot. *Phys. Rev. B* **2010**, *81*, 115324.

12. Neupane, M. R.; Rahman, R.; Lake, R. K. Carrier leakage in Ge/Si core-shell nanocrystals for lasers: core size and strain effects. *Proc. SPIE* **2011**, *8102*, 81020P–81020P–8.

13. Neupane, M. R.; Lake, R. K.; Rahman, R. Core size dependence of the confinement energies, barrier heights, and hole lifetimes in Ge-core/Si-shell nanocrystals. *Journal of Applied Physics* **2011**, *110*, 074306.

14. Neupane, M. R.; Lake, R. K.; Rahman, R. Electronic states of Ge/Si nanocrystals with crescent-shaped Ge-cores. *Journal of Applied Physics* **2012**, *112*, 5.

15. Maune, B. M.; Borselli, M. G.; Huang, B.; Ladd, T. D.; Deelman, P. W.; Holabird, K. S.; Kiselev, A. A.; Alvarado-Rodriguez, I.; Ross, R. S.; Schmitz, A. E. et al. Coherent singlet-triplet oscillations in a silicon-based double quantum dot. *Nature* **2012**, *481*, 344–347.

16. Hu, Y.; Kuemmeth, F.; Lieber, C.; M. Marcus, C. M. Hole spin relaxation in Ge-Si core-shell nanowire qubits. *Nature* **2012**, *7*, 47–50.

17. Kwon, S.; Chen, Z. C. Y.; Kim, J.-H.; Xiang, J. Misfit-Guided Self-Organization of Anticorrelated Ge Quantum Dot Arrays on Si Nanowires. *Nano Letters* **2012**, *12*, 4757–4762.

18. Gamble, J. K.; Eriksson, M. A.; Coppersmith, S. N.; Friesen, M. Disorder-induced valley-orbit hybrid states in Si quantum dots. *Phys. Rev. B* **2013**, *88*, 035310.

19. Ma, Y. J.; Zhong, Z.; Lv, Q.; Zhou, T.; Yang, X. J.; Fan, Y. L.; Wu, Y. Q.; Zou, J.;

Jiang, Z. M. Formation of coupled three–dimensional GeSi quantum dot crystals. *Applied Physics Letters* **2012**, *100*, 153113.

20. Lee, S.-W.; Chang, H.-T.; Chang, J.-K.; Cheng, S.-L. Formation Mechanism of Self-Assembled Ge/Si/Ge Composite Islands. *Journal of The Electrochemical Society* **2011**, *158*, H1113–H1116.

21. Yang, J.; Jin, Y.; Wang, C.; Li, L.; Tao, D.; Yang, Y. Evolution of self-assembled Ge/Si island grown by ion beam sputtering deposition. *Applied Surface Science* **2012**, *258*, 3637 – 3642.

22. Alkhatib, A.; Nayfeh, A. A Complete Physical Germanium-on-Silicon Quantum Dot Self-Assembly Process. *Sci. Rep.* **2013**, *3*.

23. Zhang, J.; Rastelli, A.; Schmidt, O. G.; Bauer, G. Site-controlled SiGe islands on patterned Si(001): Morphology, composition profiles, and devices. *Physica Status Solidi (b)* **2012**, *249*, 12.

24. Yakimov, A. I.; Dvurechenskii, A. V.; Proskuryakov, Y. Y.; Nikiforov, A. I.; Pchelyakov, O. P.; Teys, S. A.; Gutakovskii, A. K. Normal-incidence infrared photoconductivity in Si p-i-n diode with embedded Ge self-assembled quantum dots. *Applied Physics Letters* **1999**, *75*, 1413–1415.

25. Tayagaki, T.; Ueda, K.; Fukatsu, S.; Kanemitsu, Y. Recombination Dynamics of High-Density Photocarriers in Type-II Ge/Si Quantum Dots. *Journal of the Physical Society of Japan* **2012**, *81*, 064712.

26. Tayagaki, T.; Hoshi, Y.; Usami, N. Investigation of the open-circuit voltage in solar cells doped with quantum dots. *Sci. Rep.* **2013**, *3*.

27. Hao, X.-J.; Tu, T.; Cao, G.; Zhou, C.; Li, H.-O.; Guo, G.-C.; Fung, W. Y.; Ji, Z.;



Physical Chemistry Chemical Physics Accepted Manuscript

Physical Chemistry Chemical Physics Accepted Manuscript

Guo, G.-P.; Lu, W. Strong and Tunable Spin-Orbit Coupling of One-Dimensional Holes in Ge/Si Core/Shell Nanowires. *Nano Letters* **2010**, *10*, 2956–2960.

28. Zinovieva, A. F.; Dvurechenskii, A. V.; Stepina, N. P.; Deryabin, A. S.; Nikiforov, A. I.; Rubinger, R. M.; Sobolev, N. A.; Leitão, J. P.; Carmo, M. C. Spin resonance of electrons localized on Ge/Si quantum dots. *Phys. Rev. B* **2008**, *77*, 115319.

29. Montoro, L. A.; Leite, M. S.; Biggemann, D.; Peternella, F. G.; Batenburg, K. J.; MedeirosRibeiro, G.; Ramirez, A. J. Revealing Quantitative 3D Chemical Arrangement on Ge-Si Nanostructures. *The Journal of Physical Chemistry C* **2009**, *113*, 9018–9022.

30. McKay, M. R.; Venables, J.; Drucker, J. Kinetic frustration of Ostwald ripening in Ge/Si(100) hut ensembles. *Solid State Communications* **2009**, *149*, 1403 – 1409".

31. Cho, B.; Bareno, J.; Petrov, I.; Greene, J. E. Enhanced Ge/Si(001) island areal density and self-organization due to P predeposition. *Journal of Applied Physics* **2011**, *109*, 093526.

32. Richard, M.-I.; Schülli, T. U.; Renaud, G. In situ x-ray study of the formation of defects in Ge islands on Si(001). *Applied Physics Letters* **2011**, *99*, 161906.

33. Leite, M. S.; Kamins, T. I.; Williams, R. S.; MedeirosRibeiro, G. Intermixing during Ripening in Ge/Si Incoherent Epitaxial Nanocrystals. *The Journal of Physical Chemistry C* **2012**, *116*, 901–907.

34. Grtzmacher, D.; Fromherz, T.; Dais, C.; Stangl, J.; Mller, E.; Ekinci, Y.; Solak, H. H.; Sigg, H.; Lechner, R. T.; Wintersberger, E. et al. Three-Dimensional Si/Ge Quantum Dot Crystals. *Nano Letters* **2007**, *7*, 3150–3156, PMID: 17892317.

35. Seta, M. D.; Capellini, G.; Evangelisti, F.; Ferrari, C.; Lazzarini, L.; Salviati, G.; Peng, R. W.; Jiang, S. S. Effect of interlayer strain interaction on the island compo-

Physical Chemistry Chemical Physics Accepted Manuscript

sition and ordering in Ge/Si(001) island superlattices. *Journal of Applied Physics* **2007**, *102*, 043518.

36. Lee, S.; Chang, H.; Leeb, C.; Chengc, S.; Liu, C. Composition redistribution of self–assembled Ge islands on Si(001) during annealing. *Thin Solid Films* **2010**, *518*, S196–S199.

37. Krasilnik, Z. F.; Novikov, A. V.; Lobanov, D. N.; Kudryavtsev, K. E.; Antonov, A. V.; Obolenskiy, S. V.; Zakharov, N. D.; Werner, P. SiGe nanostructures with self–assembled islands for Si–based optoelectronics. *Semiconductor Science and Technology* **2011**, *26*, 014029.

38. Shaleev, M. V.; Novikov, A. V.; Yablonskiy, A. N.; Drozdov, Y. N.; Lobanov, D. N.; Krasilnik, Z. F.; Kuznetsov, O. A. Photoluminescence of dome and hut shaped Ge(Si) self-assembled islands embedded in a tensile-strained Si layer. *Applied Physics Letters* **2007**, *91*, 021916.

39. Mateeva, E.; Sutter, P.; Lagally, M. G. Spontaneous self-embedding of three-dimensional SiGe islands. *Applied Physics Letters* **1999**, *74*, 567–569.

40. Shaleev, M. V.; Novikov, A. V.; Yablonskiy, A. N.; Drozdov, Y. N.; Lobanov, D. N.; Krasilnik, Z. F.; Kuznetsov, O. A. Photoluminescence of Ge(Si) self-assembled islands embedded in a tensile-strained Si layer. *Applied Physics Letters* **2006**, *88*, 011914.

41. Shaleev, M.; Novikov, A.; Baydakova, N.; Yablonskiy, A.; Kuznetsov, O.; Lobanov, D.; Krasilnik, Z. Photoluminescence line width of self-assembled Ge(Si) islands arranged between strained Si layers. *Semiconductors* **2011**, *45*, 198–202, 10.1134/S1063782611020199.

42. Teherani, J. T.; Chern, W.; Antoniadis, D. A.; Hoyt, J. L.; Ruiz, L.; Poweleit, C. D.; Menéndez, J. Extraction of large valence-band energy offsets and comparison to theo-

retical values for strained-Si/strained-Ge type-II heterostructures on relaxed SiGe substrates. *Phys. Rev. B* **2012**, *85*, 205308.

43. Klenovský, P.; Brehm, M.; Křápek, V.; Lausecker, E.; Munzar, D.; Hackl, F.; Steiner, H.; Fromherz, T.; Bauer, G.; Humlíček, J. Excitation intensity dependence of photoluminescence spectra of SiGe quantum dots grown on prepatterned Si substrates: Evidence for biexcitonic transition. *Phys. Rev. B* **2012**, *86*, 115305.

44. Nenashev, A. V.; Dvurechenskii, A. V.; Zinovieva, A. F. Wave functions and $g$ factor of holes in Ge/Si quantum dots. *Phys. Rev. B* **2003**, *67*, 205301.

45. Bester, G.; Zunger, A. Cylindrically shaped zinc-blende semiconductor quantum dots do not have cylindrical symmetry: Atomistic symmetry, atomic relaxation, and piezoelectric effects. *Phys. Rev. B* **2005**, *71*, 045318.

46. Pizzi, G.; Virgilio, M.; Grosso, G. Tight-binding calculation of optical gain in tensile strained [001]-Ge/SiGe quantum wells. *Nanotechnology* **2010**, *21*, 055202.

47. Skoulidis, N.; Polatoglou, H. Modeling the optical properties of Si-capped germanium quantum dots. *Computational Materials Science* **2005**, *33*, 303 – 309.

48. Julsgaard, B.; Balling, P.; Hansen, J. L.; Svane, A.; Larsen, A. N. Luminescence decay dynamics of self-assembled germanium islands in silicon. *Applied Physics Letters* **2011**, *98*, 093101.

49. Lavchiev, V. M.; Schade, U.; Hesser, G.; Chen, G.; Jantsch, W. Ellipsometry and spectroscopy on 1.55 $\mu$m emitting Ge islands in Si for photonic applications. *Phys. Rev. B* **2012**, *86*, 125421.

50. Usman, M.; Heck, S.; Clarke, E.; Spencer, P.; Ryu, H.; Murray, R.; Klimeck, G. Experimental and theoretical study of polarization-dependent optical transitions in InAs



Physical Chemistry Chemical Physics Accepted Manuscript

quantum dots at telecommunication-wavelengths (1300–1500 nm). *Journal of Applied Physics* **2011**, *109*, 104510.

51. Usman, M.; Tan, Y.-H. M.; Ryu, H.; Ahmed, S. S.; Krenner, H. J.; Boykin, T. B.; ; Klimeck, G. Quantitative excited state spectroscopy of a single InGaAs quantum dot molecule through multi–million–atom electronic structure calculations. *Nanotechnology* **2011**, *22*.

52. Usman, M. In-plane polarization anisotropy of ground state optical intensity in InAs/GaAs quantum dots. *Journal of Applied Physics* **2011**, *110*, 094512.

53. Zhou, H.; Gann, R.; Li, B.; Liu, J.; Yarmoff, J. A. Performance enhancement of $TiSi_2$ coated Si nanocrystal memory device. Mater. Res. Soc. Symp. 2009.

54. Zhou, H.; Li, B.; Yang, Z.; Zhan, N.; Yan, D.; Lake, R. K.; Liu, J. $TiSi_2$ Nanocrystal Metal Oxide Semiconductor Field Effect Transistor Memory. *IEEE Trans. on Nanotechnology* **2011**, *10*, 499 – 505.

55. Tonkikh, A.; Zakharov, N.; Talalaev, V.; Werner, P. Ge/Si(100) quantum dots grown via a thin Sb layer. *physica status solidi (RRL) Rapid Research Letters* **2010**, *4*, 224–226.

56. Yakimov, A.; Nikiforov, A.; Bloshkin, A.; Dvurechenski, A. Electromodulated reflectance study of self-assembled Ge/Si quantum dots. *Nanoscale Research Letters* **2011**, *208*, 136602.

57. Klenovský, P.; Brehm, M.; Křápek, V.; Lausecker, E.; Munzar, D.; Hackl, F.; Steiner, H.; Fromherz, T.; Bauer, G.; Humlíček, J. Excitation intensity dependence of photoluminescence spectra of SiGe quantum dots grown on prepatterned Si substrates: Evidence for biexcitonic transition. *Phys. Rev. B* **2012**, *86*, 115305.

58. Yuryev, V.; Arapkina, L.; Storozhevykh, M.; Chapnin, V.; Chizh, K.; Uvarov, O.; Kalinushkin, V.; Zhukova, E.; Prokhorov, A.; Spektor, I. et al. Ge/Si(001) heterostructures



Physical Chemistry Chemical Physics Accepted Manuscript

Physical Chemistry Chemical Physics Accepted Manuscript

with dense arrays of Ge quantum dots: morphology, defects, photo-emf spectra and terahertz conductivity. *Nanoscale Research Letters* **2012**, *7*, 414.

59. Liu, Z.; Hu, W.; Su, S.; Li, C.; Li, C.; Xue, C.; Li, Y.; Zuo, Y.; Cheng, B.; Wang, Q. Enhanced photoluminescence and electroluminescence of multilayer GeSi islands on Si(001) substrates by phosphorus-doping. *Opt. Express* **2012**, *20*, 22327–22333.

60. Yakimov, A. I.; Mikhalyov, G. Y.; Dvurechenskii, A. V.; Nikiforov, A. I. Hole states in Ge/Si quantum-dot molecules produced by strain-driven self-assembly. *Journal of Applied Physics* **2007**, *102*, 093714.

61. Rastelli, A.; Müller, E.; von Känel, H. Shape preservation of Ge/Si(001) islands during Si capping. *Applied Physics Letters* **2002**, *80*, 1438–1440.

62. Baranov, A. V.; Fedorov, A. V.; Perova, T. S.; Moore, R. A.; Yam, V.; Bouchier, D.; Le Thanh, V.; Berwick, K. Analysis of strain and intermixing in single-layer Ge/Si quantum dots using polarized Raman spectroscopy. *Phys. Rev. B* **2006**, *73*, 075322.

63. Ogawa, Y.; Toizumi, T.; Minami, F.; Baranov, A. V. Nanometer-scale mapping of the strain and Ge content of Ge/Si quantum dots using enhanced Raman scattering by the tip of an atomic force microscope. *Phys. Rev. B* **2011**, *83*, 081302.

64. Klimeck, G.; Ahmed, S.; Bae, H.; Kharche, N.; Clark, S.; Haley, B.; Sunhee,; Naumov, M.; Ryu, H.; Saied, F. et al. Atomistic Simulation of Realistically Sized Nanodevices Using NEMO 3-D Part I– Models and Benchmarks. *IEEE Transactions on Electron Devices* **2007**, *54*, 2090 – 2099.

65. Kharche, N.; Prada, M.; Boykin, T. B.; Klimeck, G. Valley splitting in strained silicon quantum wells modeled with $2^o$ miscuts, step disorder, and alloy disorder. *Applied Physics Letters* **2007**, *90*, 092109.

66. Ryu, H.; Lee, S.; Weber, B.; Mahapatra, S.; Hollenberg, L. C. L.; Simmons, M. Y.; Klimeck, G. Atomistic modeling of metallic nanowires in silicon. *Nanoscale* **2013**, *5*, 8666–8674.

67. Rahman, R.; Wellard, C. J.; Bradbury, F. R.; Prada, M.; Cole, J. H.; Klimeck, G.; Hollenberg, L. C. L. High Precision Quantum Control of Single Donor Spins in Silicon. *Phys. Rev. Lett.* **2007**, *99*, 036403.

68. Lansbergen, G. P.; Rahman, R.; Wellard, C. J.; Caro, J.; Collaert, N.; Biesemans, S.; Klimeck, G.; Hollenberg, L. C. L.; Rogge, S. Gate-induced quantum-confinement transition of a single dopant atom in a silicon FinFET. *Nature* **2008**, *4*, 656–661.

69. Weber, B.; Mahapatra, S.; Ryu, H.; Lee, S.; Fuhrer, A.; Reusch, T. C. G.; Thompson, D. L.; Lee, W. C. T.; Klimeck, G.; Hollenberg, L. C. L. et al. Ohms Law Survives to the Atomic Scale. *Science* **2012**, *335*, 64–67.

70. Büch, H.; Mahapatra, S.; Rahman, R.; Morello, A.; Simmons, M. Y. Spin readout and addressability of phosphorus-donor clusters in silicon. *Nat Commun* **2013**, *4*.

71. Pryor, C.; Kim, J.; Wang, L. W.; Williamson, A. J.; Zunger, A. Comparison of two methods for describing the strain profiles in quantum dots. *Journal of Applied Physics* **1998**, *83*, 2548–2554.

72. Klimeck, G.; Oyafuso, F.; Boykin, T. B.; Bowen, R. C.; von Allmen, P. Development of a Nanoelectronic 3-D (NEMO 3-D ) Simulator for Multimillion Atom Simulations and Its Application to Alloyed Quantum Dots. *CMES* **2002**, *3*, 601–642.

73. Oyafuso, F.; Klimeck, G.; Allmen, P.; Boykin, T.; Bowen, R. Strain Effects in large-scale atomistic quantum dot simulations. *physica status solidi (b)* **2003**, *239*, Phys. Stat. Sol. (b), Vol. 239, p 71-79 (2003); doi: 10.1002/pssb.200303238.




Physical Chemistry Chemical Physics Accepted Manuscript

74. Paul, A.; Luisier, M.; Klimeck, G. Modified valence force field approach for phonon dispersion: from zinc-blende bulk to nanowires. *Journal of Computational Electronics* **2010**, *9*, 160–172.

75. Boykin, T. B.; Klimeck, G.; Bowen, R. C.; Oyafuso, F. Diagonal parameter shifts due to nearest-neighbor displacements in empirical tight-binding theory. *Phys. Rev. B* **2002**, *66*, 125207.

76. Lee, S.; Oyafuso, F.; von Allmen, P.; Klimeck, G. Boundary conditions for the electronic structure of finite-extent embedded semiconductor nanostructures. *Phys. Rev. B* **2004**, *69*, 045316.

77. Rahman, R.; Park, S. H.; Cole, J. H.; Greentree, A. D.; Muller, R. P.; Klimeck, G.; Hollenberg, L. C. L. Atomistic simulations of adiabatic coherent electron transport in triple donor systems. *Phys. Rev. B* **2009**, *80*, 035302.

78. Salfi, J.; Mol, J. A.; Rahman, R.; Klimeck, G.; Simmons, M. Y.; Hollenberg, L. C. L.; Rogge, S. Spatially resolving valley quantum interference of a donor in silicon. *Nature Materials* **2014**, *13*, 605 – 610.

79. Naumov, M.; Lee, S.; Haley, B.; Bae, H.; Clark, S.; Rahman, R.; Ryu, H.; Saied, F.; Klimeck, G. Eigenvalue solvers for atomistic simulations of electronic structures with NEMO-3D. *Journal of Computational Electronics* **2008**, *7*, 297–300.

80. Boykin, T. B.; Klimeck, G.; Oyafuso, F. Valence band effective-mass expressions in the $sp^3d^5s^*$ empirical tight-binding model applied to a Si and Ge parametrization. *Phys. Rev. B* **2004**, *69*, 115201.

81. Boykin, T. B.; Kharche, N.; Klimeck, G. Brillouin-zone unfolding of perfect supercells having nonequivalent primitive cells illustrated with a Si/Ge tight-binding parameterization. *Phys. Rev. B* **2007**, *76*, 035310.



Physical Chemistry Chemical Physics Accepted Manuscript

82. Ryu, H.; Nam, D.; Ahn, B.-Y.; Lee, J. R.; Cho, K.; Lee, S.; Klimeck, G.; Shin, M. Optical {TCAD} on the Net: A tight-binding study of inter-band light transitions in self-assembled InAs/GaAs quantum dot photodetectors. *Mathematical and Computer Modelling* **2013**, *58*, 288 – 299.

83. Wang, K.; Payette, C.; Dovzhenko, Y.; Deelman, P. W.; Petta, J. R. Charge Relaxation in a Single-Electron Si/SiGe Double Quantum Dot. *Phys. Rev. Lett.* **2013**, *111*, 046801.

84. Talochkin, A. B.; Markov, V. A.; Mashanov, V. I. Inelastic strain relaxation in the Ge quantum dot array. *Applied Physics Letters* **2007**, *91*, 093127.

85. Zheng, Y.; Rivas, C.; Lake, R.; Alam, K.; Boykin, T. B.; Klimeck, G. Electronic properties of silicon nanowires. *IEEE Trans. Elect. Dev.* **2005**, *52*, 1097–1103.

86. Walle, G. G. D. Band lineups and deformation potentials in the model-solid theory. *Phys. Rev. B* **1989**, *39*, 1871 – 1883.

Physical Chemistry Chemical Physics Accepted Manuscript